Highlights

Modeling motor-evoked potentials from neural field simulations of transcranial magnetic stimulation

Marcus T Wilson, Bahar Moezzi, Nigel C Rogasch

- A model of motor-evoked potential formation gives a realistic electromyogram in response to TMS.
- The model reproduces effects of SICI, ICF and LICI.
- A link between existing neural field modeling and realistic outcome measures of TMS is provided.

Modeling motor-evoked potentials from neural field simulations of transcranial magnetic stimulation

Marcus T Wilson[a], Bahar Moezzi[b], Nigel C Rogasch[c]

[a]*School of Science, University of Waikato, Hamilton, New Zealand*
[b]*Cognitive Ageing and Impairment Neurosciences Laboratory, School of Psychology, Social Work and Social Policy, The University of South Australia, Australia*
[c]*Discipline of Psychiatry, Adelaide Medical School, University of Adelaide, Australia; South Australian Health and Medical Research Institute, Australia; Brain, Mind and Society Research Hub, The School of Psychologcial Sciences, The Turner Institute for Brain and Mental Health and Monash Biomedical Imaging, Monash University, Australia.*

Abstract

Introduction: Understanding how transcranial magnetic stimulation (TMS) interacts with cortical circuits is enhanced through biophysical modeling. Existing population-based models of TMS-evoked activity and plasticity evaluate changes in cortical synaptic weights. However, it remains unclear how these changes impact motor-evoked potentials (MEPs), an experimental measure inferring the cortical response to TMS.

Objectives: To develop a population-based biophysical model of MEPs following TMS.

Methods: We combined an existing MEP model with population-based cortical modeling. Layer 2/3 excitatory and inhibitory neurons are stimulated with TMS and feed layer 5 corticospinal neurons, which also couple directly but weakly to the TMS pulse. The layer 5 output controls mean motoneuron responses, which generate a series of single motor-unit action potentials that are summed to estimate a MEP.

Results: A MEP waveform was generated comparable to those observed experimentally. The model captured TMS phenomena including a sigmoidal input-output curve, common paired pulse effects (SICI, ICF, LICI) including responses to pharmacological interventions, and a cortical silent period. Changes in MEP amplitude following theta burst paradigms were observed including variability in outcome direction.

Conclusions: Better interpretation of population-based TMS modeling

approaches is achieved by interpreting output via MEPs, providing a quantitative link between theoretical models and experimental outcomes.

Keywords: Motor Evoked Potential, MEP, Transcranial Magnetic Stimulation, TMS, corticomotor system, cortical plasticity, modeling, neural field theory, paired-pulse, rTMS, calcium dependent plasticity, iTBS, cTBS, theta burst stimulation

1. Introduction

Transcranial Magnetic Stimulation (TMS) is a non-invasive form of brain stimulation used for the study of brain function and for clinical treatments of brain disorders such as depression [1, 2, 3, 4]. Applying a single TMS pulse at sufficient intensity over the primary motor cortex results in firing of layer 5 corticospinal neurons due to both transsynaptic activation from layer 2/3 interneurons and horizontal fibres, and direct activation of the neurons by the pulse. The descending volley of activity gives a measurable motor response in peripheral muscles targeted by the stimulated region, known as a motor-evoked potential (MEP). MEPs have been widely used as a measure of the excitability of the corticomotor system in TMS studies, and have revealed several well known neural phenomena related to TMS, such as periods of net inhibition and excitation following paired pulse protocols (i.e. short and long interval intracortical inhibition [SICI; LICI], and intracortical facilitation [ICF]), and a cortical silent period observed when TMS is given during a voluntary contraction. Furthermore, MEPs are used to assess changes in cortical excitability resulting from repetitive TMS (rTMS) protocols, which are thought to induce plasticity in cortical circuits through mechanisms similar to long-term potentiation and depression (LTP/D). However, despite nearly 30 years of research, it remains unclear how microscale mechanisms underlying plasticity occurring at synaptic level (e.g. LTP/D) manifest when large populations of neurons are activated as with TMS [5, 6].

Biophysically-informed models provide a mathematical description of TMS and other neurostimulation effects that can be used to better understand TMS phenomena [7]. Models typically describe biophysical processes with equations. Existing models include descriptions of the shape and timecourse of the magnetic and induced electric fields due to TMS, including realistic human head geometries [8, 9, 10, 11, 12], descriptions of spiking of single neurons and small networks of neurons, for example I-waves [13, 14], population-based

descriptions of neural firing rates [15, 16] and plasticity effects [17, 18].

While the formation of a MEP involves highly nonlinear processes, including electrical propagation along nerve pathways and motounit responses, the modeling of these need not be complicated. Li *et al.* [19] have described a MEP amplitude and shape in terms of a sum of individual motor unit responses, with thresholds for the motor units distributed exponentially. Rusu *et al.* [13] and then Moezzi *et al.* [14] have developed this further; they have modeled I-wave and MEP formation following TMS using a population of layer 2/3 excitatory and inhibitory neurons, feeding layer 5 cortical cells and motoneurons. They reproduced I-waves and MEP-responses that matched closely those measured experimentally. In contrast, Goetz have used a statistical model based on experimental data to compile a MEP model [20].

Cortical plasticity, a lasting change in strengths of connections between neurons, has been modeled using population-based measures of activity [21, 17, 22, 18]. In these works, plasticity has been included using rules which capture either phenomenological descriptions of plasticity (e.g. spike timing dependent plasticity), or physiological theories (e.g. calcium dependent plasticity). Population-based modeling [15, 16], including neural mass or neural field approaches, is well suited to TMS because a TMS pulse excites many thousands of neurons over an area of several centimeters-squared. However, population-based cortical modeling of TMS has been hard to interpret in relation to human experiments. For example, most models have evaluated changes in synaptic weights between excitatory neural populations following rTMS but it remains unclear how these changes would impact the amplitude of MEPs.

We have simplified the approach of Moezzi *et al.* [14] by modeling the layer 2/3 and layer 5 populations with population-based dynamics. Firing rates of motoneurons are described as functions of the layer 5 firing rate, and a train of motoneuron firings is reconstructed. Thus MEP activity is determined. This approach provides a much-needed link between population-based models of cortical dynamics, and models of MEP activity, thereby allowing a direct comparison between model outputs and human experiments. To test the generalisability of our MEP model, we first assess whether we can capture well known single and paired-pulse MEP phenomena. We then evaluate how sensitive our MEP model is to changes in synaptic weights predicted by population-based rTMS models of plasticity.

2. Methods

We have combined a neural field approach [22, 18] with existing models of MEP formation [19, 14]. The scheme is shown schematically in Fig. 1.

2.1. Neural Field components

Neural Field Theory (NFT) provides a nonlinear, statistical model for the dynamics of populations of neuronal cells and their interactions via dendrites and axons [15, 16, 25, 26, 27]. Population-averaged properties such as mean firing rate and axonal pulse rate are modeled as a function of time t. We have used the NFTsim model [23]. The mathematical description and parameter values are summarized in the appendix.

Specifically, a population of layer 2/3 excitatory neurons (labeled 'e), a population of layer 2/3 inhibitory neurons (i), and a population of layer 5 excitatory cortical neurons (v) are modeled with NFTSim. These populations couple together as indicated by the arrows in Fig. 1. They are also coupled to an external driving population (labeled x) describing the TMS application. Coupling strengths *to* population a *from* population a are denoted in this paper by ν_{ab}, where a and b can take the labels e, i, x or v. Synaptic responses include both fast-acting $\mathrm{GABA_A}$ and slower-acting $\mathrm{GABA_B}$ effects [18, 7].

Simulating pulse lengths are chosen to be 0.5 ms. In NFTsim, stimulation is applied with an 'external' rate $\phi_x(t)$ [17], which can be interpreted as average number of action potentials per second that are introduced along each axon in the cortical populations. For example, a stimulus intensity of $1000\ \mathrm{s}^{-1}$ for 0.5 ms introduces on average 0.5 action potential onto each axon.

The strength of this drive depends upon the TMS intensity — low intensities preferentially stimulate the inhibitory neurons over the excitatory neurons, but at higher intensities, the excitatory neurons are strongly stimulated [28]. To achieve this, we keep constant the external TMS to inhibitory cell coupling, at $\nu_{ix} = -1.15 \times 10^{-4}$ V s. The external TMS to layer 2/3 excitatory coupling is changed as a function of stimulus intensity ϕ_x with a sigmoid relationship:

$$\nu_{ex} = \frac{\nu_{ex}^{\max}}{e^{(A-\phi_x)/B} + 1} \tag{1}$$

where $\nu_{ex}^{\max} = 1.92 \times 10^{-4}$ V s is the maximum external to layer 2/3 excitatory coupling, with $A = 500\ \mathrm{s}^{-1}$ and $B = 100\ \mathrm{s}^{-1}$ describing the threshold and width of the curve respectively.

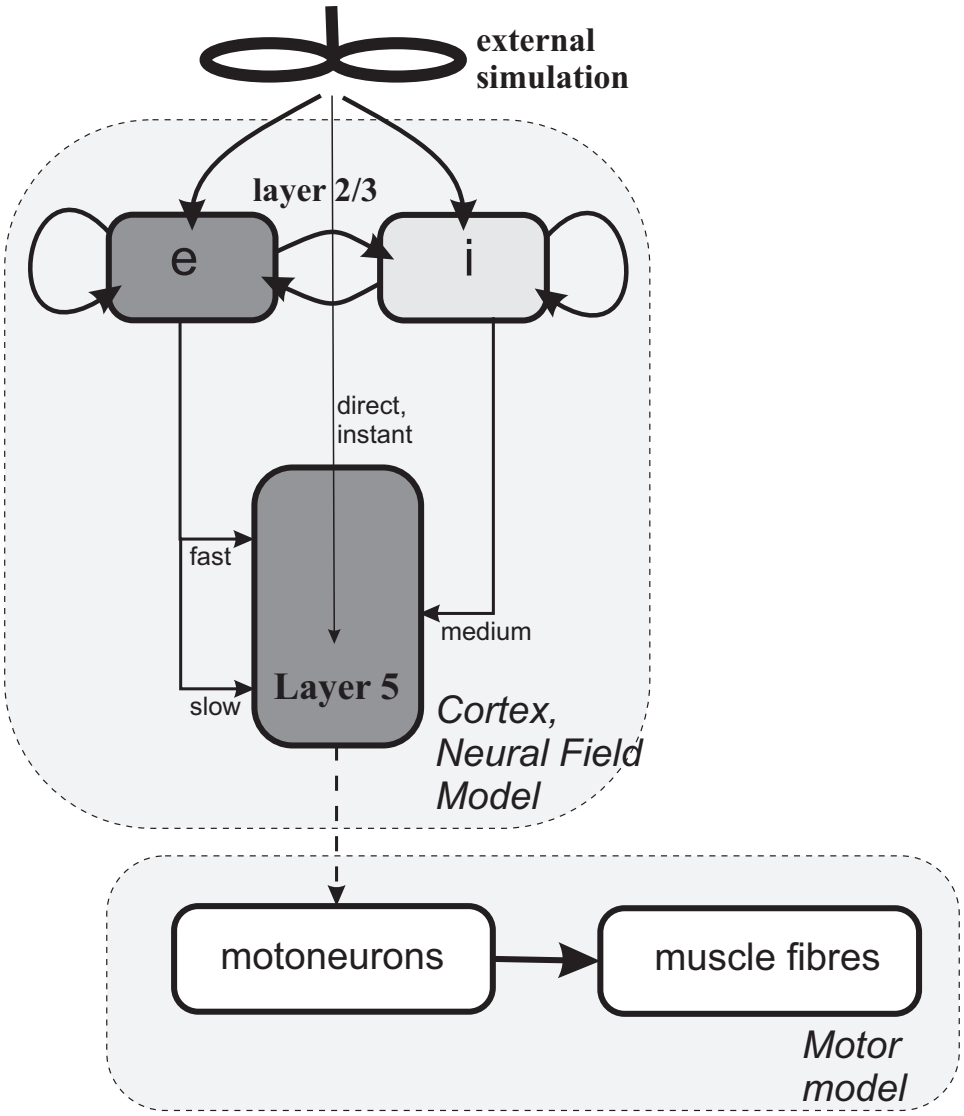

Figure 1: A schematic of the modeling approach. TMS stimulates populations of layer 2/3 excitatory and inhibitory neurons. The layer 2/3 populations stimulate each other. They have multiple projections to a population of layer 5 excitatory which also receive low-intensity direct stimulation from the TMS pulses. These three are modeled with NFTsim [23]. The axonal flux from the layer 5 cells stimulates a population of motoneurons within the spinal cord; each motoneuron firing produces a response from the muscle fibres. The sum of these fibre responses produces a MEP. The latter components are modeled with the approach of Li *et al.* [24].

The layer 2/3 populations project to a population of layer 5 excitatory cortical neurons (v). There are multiple projections to different parts of the dendritic tree. Excitatory connections are made with short and long propagation delays (specifically 1 ms and 5 ms respectively), to model connections far from and close to the soma. Inhibitory connections are made with a medium time delay (specifically 3 ms) [13, 14]. Additionally, the layer 5 population is excited directly from the TMS stimulation at a low strength of $\nu_{vx} = 0.1\nu_{ex}$ to account for the layer 5 cells receiving a much lower electromagnetic field intensity than the layer 2 and 3 cells [14].

The layer 2/3 excitatory, layer 2/3 inhibitory and layer 5 populations plus the external stimulation are modeled with NFTsim [23]. Although there are many parameters, many have physical constraints placed on them [29]. Parameters for the layer 2 and 3 cells have been chosen to be consistent with previous modeling [18, 30]; for the layer 5 cells the firing response to synaptic input has been tuned to give plausible responses to stimulation, broadly consistent with Moezzi *et al.* [14], including maximum population firing rate of 300 s^{-1} and a rapid climb in output once threshold has been reached at a mid-range stimulation intensity.

The NFT modeling gives the mean axonal flux rate of the layer 5 neural population as a function of time. This firing rate is then used as an input (dotted arrow in Fig. 1) to the next stage of modeling, summarized by the lower gray box in the figure.

TMS stimulation of the cortex can lead to both direct (D-) and indirect (I-) waves of descending activity, recorded in the epidural space [1, 31]. Often several indirect waves are recorded, at several hundred hertz frequency. While their origin has not been precisely established, they are likely to be a result of TMS-induced activity within the cortex propagating down nerve pathways. Rusu *et al.* presented a simple model of I-wave formation by projecting populations of layer 2 and 3 cells onto a compartmentalized layer 5 neuron [13]. Averaged responses of many cases showed synchrony in layer 5 firings, resulting in I-waves of activity. Moezzi et al. has demonstrated similar synchrony by modeling explicitly many layer 5 cells simultaneously [14]. In our model it is not possible to capture I-waves in a similar way, since neural synchrony is not explicitly captured when only population-averaged rates are considered because exact timings of firings are not explicitly modeled [7, 32]. That is, a mean firing rate of a population does not tell us about the synchrony of firings within the population. While the population approach is not well-suited to capturing firing events such as those generat-

ing I-waves, it is well suited for capturing the slower shifts in net excitation and inhibition which are thought to underlie paired-pulse phenomena such as SICI and ICF.

2.2. MEP model components

Population-averaged cortical responses are often linear or nearly-linear, making NFT appropriate [15, 32]. However, motor responses are challenging to describe in a linear way; for example 20 motoneurons firing at 100 s^{-1} produces a very different MEP to 10 motoneurons firing at 200 s^{-1}.

Instead, we use a model of Li *et al.* [19] to describe MEP formation. Here, the layer 5 axonal pulse rate ϕ_v is used to determine the rate of firing of $N = 100$ motoneurons. Each motoneuron, indexed by k, has an instantaneous firing rate Q_k ($k = 1 \cdots N$) that is a function of the axonal flux rate from the layer 5 cells [19], that is $Q_k = f_k(\phi_v)$.

All motoneurons have a threshold input below which they do not fire. Thresholds are distributed exponentially:

$$T_k = T_{\min} e^{\alpha k} \tag{2}$$

where T_k is the threshold of the k-th unit and $T_{\min}$ is a minimum threshold (set to 14 s^{-1} [19]). The parameter α dictates the range R of possible thresholds, through $\alpha = \ln R/N$. When the axonal flux rate ϕ_v from the layer 5 neurons exceeds a unit's threshold T_k, the unit fires with a rate given by the following function of axonal flux:

$$Q_k(t) = f_k(\phi_v(t)) = q + \kappa_k(\phi_v(t) - T_k) \tag{3}$$

where q is the minimum firing rate (which we set at 8 Hz for all units) and κ_k is a constant for each k. The gradient κ_k is chosen separately for each k so that all motoneurons reach the same Q_k when ϕ_v is equal to $Q_v^{\max}$, the maximum firing rate of the layer 5 neurons. We set $Q_v^{\max}$, to 300 s^{-1}, to broadly align with previous simulations at high (150% resting motor threshold, RMT) pulse intensity [14].

We next determine the times at which the motoneurons fire. For the k-th motoneuron, we find firing times τ_k^j, where the superscript j denotes the j-th firing event of the k-th unit, by time-integrating $Q_k(t)$ [32]; when it passes an integer, j, we identify a firing event. That is, the τ_k^j obey:

$$\int_{t=t_0}^{\tau_k^j} Q_k(t)dt = j, \tag{4}$$

where t_0 is the time that the firing rate of the neuron crosses its threshold value.

We produce a MEP by summing individual motounit action potentials (MUAPs). Each motoneuron leads to a MUAP whose size M_k is proportional to its threshold — that is, the units recruited latest fire the strongest. Thus $M_k = M_0 e^{\alpha k}$, where M_0 is a constant set to be 42 mV s^{-1} so that the MEP's amplitude is around 2 mV for pulses at 150% RMT at a low background activation rate [33, 1, 34]. The shape of the MUAP is described by a first order Hermite-Rodriguez function $H(t)$ [19, 14, 35]:

$$H(t) = -te^{-\left(\frac{t}{\lambda}\right)^2}, \tag{5}$$

where λ is a constant timescale which we set at 2.0 ms [19]. Thus, an electromyogram (EMG) response, $M(t)$, is given by the sum of the contributions from the various MUAPs:

$$M(t) = \sum_{jk} M_k H(t - \tau_k^j) \tag{6}$$

We define a MEP as the maximum positive deflection plus the maximum negative deflection.

We mostly used standard parameter values to match Li *et al.* [19], but have adjusted slightly the MUAP amplitude M_0 and the minimum threshold $T_{\min}$ to give very limited EMG activity with no voluntary contraction. In simulating response curves we used a range of parameters. We vary the following by 15% upwards and downwards: motoneuron threshold $T_{\min}$ to account for motounit variation; layer 5 threshold θ_v to account for variations in layer 5 cells; excitatory-to-excitatory coupling in layer 2/3, ν_{ee}, to account for inter-individual variation in cortical connectivity; and TMS-to-excitatory coupling ν_{ex} to account for variable stimulation strength at the cortical surface.

2.3. Application to single- and paired-pulse protocols

To evaluate how well our model captures TMS-evoked activation of the corticomotor system, we assessed the models capacity to generate TMS-related phenomena. First we assessed how the modeled MEP changed with increasing TMS intensities (i.e. an input-output curve). Typically, MEPs increase in sigmoid shape, reaching a plateau above ∼180% RMT.

Second, we assessed how the MEP was modulated following paired pulse paradigms. A sub- or suprathreshold conditioning TMS pulse was delivered followed by a test TMS pulse after a given inter-stimulus interval. The peak-to-peak amplitude of the conditioned MEP is then compared against a MEP following a test TMS pulse alone (i.e. an unconditioned MEP). Subthreshold conditioning pulses are followed by a period of inhibition lasting 1-6 ms (short-interval intracortical inhibition, SICI) and then a period of facilitation lasting 10–15 ms (intracortical facilitation, ICF). Suprathreshold conditioning pulses are followed by strong facilitation which peaks at $\sim$20 ms, and then a long period of inhibition lasting 50–200 ms (long-interval intracortical inhibition, LICI). SICI and ICF are modulated by drugs which target $GABA_A$ and NMDA receptors, whereas LICI is modulated by drugs targeting $GABA_B$ receptors. To test this, we modulated the parameters governing $GABA_A$, $GABA_B$ and excitatory (time constant equivalent to NMDA receptors) synaptic coupling and assessed their impact on SICI, ICF and LICI.

Finally, we assessed how the modeled MEP was altered with a tonic muscle contraction. MEPs increase in amplitude with increasing voluntary muscle activation, and are followed by a cessation in muscle activity which last for 200-300 ms and is known as the cortical silent period (CSP). To model a tonic contraction, we introduced a small constant rate of 0.5 s^{-1} for each %MVC [14] to the external stimulation population.

2.4. Application to repetitive TMS protocols

A central motivation for developing a MEP model of TMS was to provide a more realistic output measure for neural field models of plasticity induced by repetitive TMS (rTMS) protocols. As a proof-of-concept, we assessed how modeled MEPs were altered following either intermittent or continuous theta burst stimulation (iTBS, cTBS). We included features of calcium-dependent plasticity with a Bienenstock-Cooper-Munro (BCM) rule for metaplasticity [22, 18, 7], see the appendix. We and others have previously demonstrated that this plasticity model captures several key features of TBS-induced plasticity by assessing changes in synaptic weights following stimulation (e.g. synaptic weights are increased following iTBS and decreased following cTBS). However, it remains unclear how these changes in synaptic weights would impact MEP amplitude.

We simulated canonical cTBS and iTBS protocols with three pulses per burst at 50 Hz intraburst rate, five bursts per second, for a total of 600 pulses.

For cTBS pulses were applied continuously; for iTBS pulses were applied for 2 s then were absent for 8 s, before repeating. Stimulation was applied at 80% of RMT. MEPs were modeled before and after TBS at a stimulation intensity of 120% of the pre-TBS RMT.

Although initial experimental studies suggested that iTBS increased, whereas cTBS decreased, MEP amplitude, more recent studies have suggested that response to TBS is variable across individuals. The variability likely arises from both methodological and biological factors. For instance, Hamada *et al.* [36] found that the manner of interaction of TMS with cortical circuits was associated with the direction of change in MEPs following iTBS and cTBS. In contrast, Mori *et al.* [37] found that single nucleotide polymorphisms in genes associated with glutamatergic NMDA receptors impacted iTBS outcomes. To assess the impact of methodological and biological variability on TBS-induced changes in MEPs, we altered the synaptic coupling of TMS to the layer 2/3 excitatory population to mimic variability in how TMS interacts with cortical circuits, and the parameter governing synaptic coupling between layer 2/3 excitatory populations to mimic variability in glutamatergic receptors.

3. Results

3.1. Motor evoked potential at rest

A simulated EMG at rest is shown in Fig. 2. A stimulation intensity of 780 s^{-1} (120% RMT) has been used with a pulse length of 0.5 ms [18]. Part (a) gives a plot of the EMG as a function of time (stimulation is at 0 s); the MEP is indicated. The corresponding layer 5 pulse rate is shown in part (b), and the firings of motoneurons are shown in part (c). Each dot corresponds to a firing of a unit arranged such that the lowest threshold firings correspond to the lowest-indexed units. The MEP demonstrates a realistic shape, with a rapid positive rise about 25 ms after the TMS pulse, followed by rapid fall to a maximum negative deflection about 10 ms later. Small amplitude activity follows the pulse.

Figure 2(b) shows the mean pulse rate, relative to the baseline of 17.8 s^{-1}. Initially, around 2 ms after the initial TMS pulse, there is a small (40 s^{-1}) peak in the response. This time delay for layer 5 response compares reasonably with the 2 to 3 ms of Moezzi *et al.* [14] and is similar to experiment (1.5–2 ms) [1].

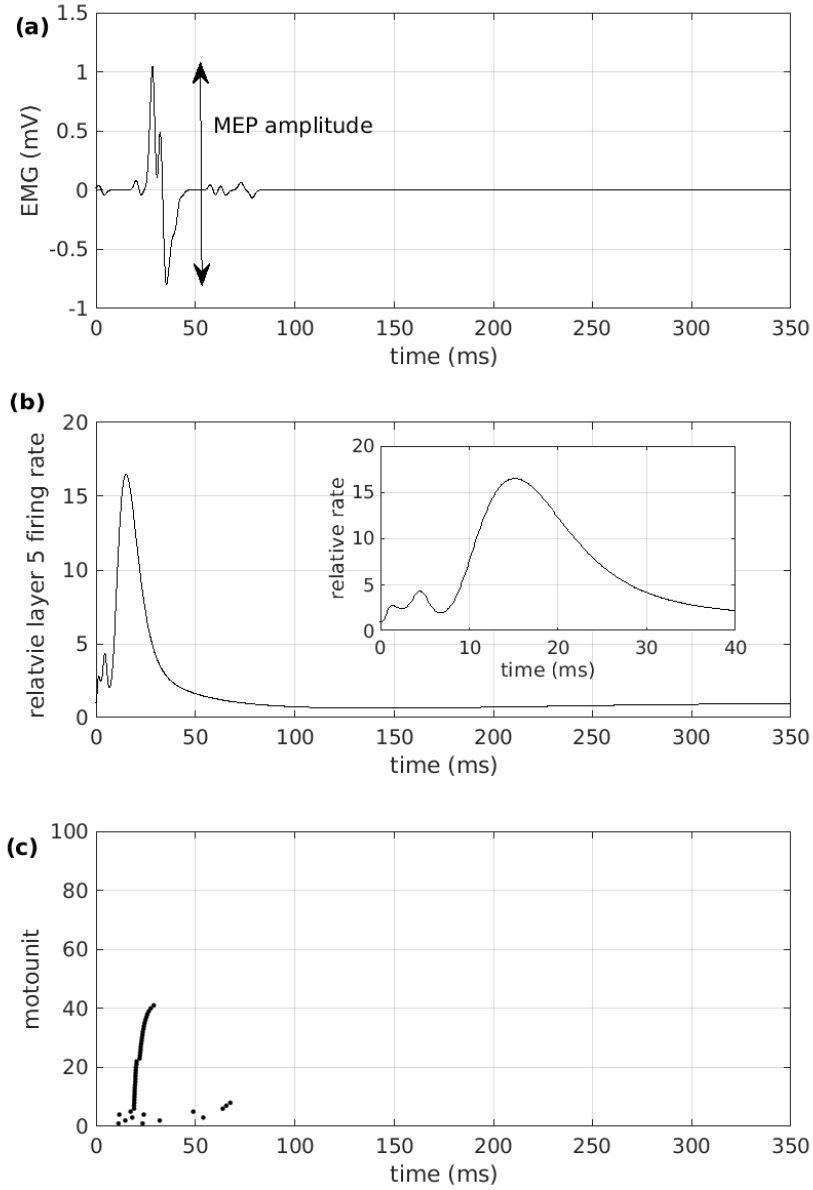

Figure 2: (a) A typical EMG produced by the model as a function of time. The MEP is indicated. The TMS pulse occurs at 0 s. (b) The mean rate of firing of the layer 5 population as a function of time, for various intensities of stimulation, plotted relative to the baseline rate. The inset shows an enlarged version at early times. (c) Motoneuron firings as a function of time.

There are further peaks of activity. A peak of 80 s^{-1} occurs at 5 ms after stimulation, and a peak of nearly 300 s^{-1} at 15 ms. Examination of the modeled cortical responses shows that these peaks are a result of indirect stimulation of the layer 5 cells, via the excitatory layer 2/3 cells. There is a strong dip before the final peak, due to build-up of $GABA_A$ inhibitory effects after the initial rise, but it is short-lived. After about 15 ms, the layer 5 neurons reach a maximum firing rate. Beyond this time, there is a drop-off in activity as the longer timescale $GABA_B$ inhibitory neurotransmitter effects become prevalent. Since Fig. 2(b) shows mean activity across a population, the peaks and troughs of the plot should not be considered as the I-waves *per se*; rather we may expect such waves to be possible during the times where the activity is large. Changes in layer 5 firing rate are consistent with recent invasive recordings in rodents [24] and non-human primates [38].

The firings of the motoneurons are shown in Fig. 2(c).

The effect of TMS intensity on MEP amplitude is shown in Fig. 3. From this plot we identify a resting motothreshold of about 650 s^{-1} input intensity, as being the amplitude that gives a MEP of around 0.1 mV. There is considerable variation in maximum output intensity, from about 1 – 7 mV. However, there is more consistency in threshold; all responses are very low at 600 /s and then climb rapidly with stimulation intensity. By 1200 s^{-1} stimulation (approx 180% RMT) most responses have flattened.

3.2. Paired-pulse protocols

To model SICI and ICF we have applied a conditioning stimulus at 70% RMT and a test stimulus at 120% RMT. The interstimulus interval (ISI) has been varied up to 20 ms. Results are shown in Fig. 4(a). For short ISI (5 ms or less) there is substantial inhibition of the pulse; at very short ISI the response to the test pulse is almost abolished. This broadly agrees with experiment (shown for comparison) which demonstrates that SICI at subthreshold conditioning intensities persists up to approximately 7 ms ISI [39]. At longer ISI (7 ms and greater) the model shows facilitation of the test pulse. This facilitation peaks at about 10 ms, in agreement with experiment [40, 39, 33].

Modeling of LICI is achieved by pairing two suprathreshold pulses at 120% RMT. Results are shown in Fig. 4(b) and the experimental plot of [40] is shown for comparison. At ISI less than 50 ms there is substantial facilitation of the test pulse, but at longer ISI (50 ms to 300 ms) there is considerable inhibition. While broadly consistent with experiment there are some differences. First, the extent of the ICF is higher than usually seen, and the period

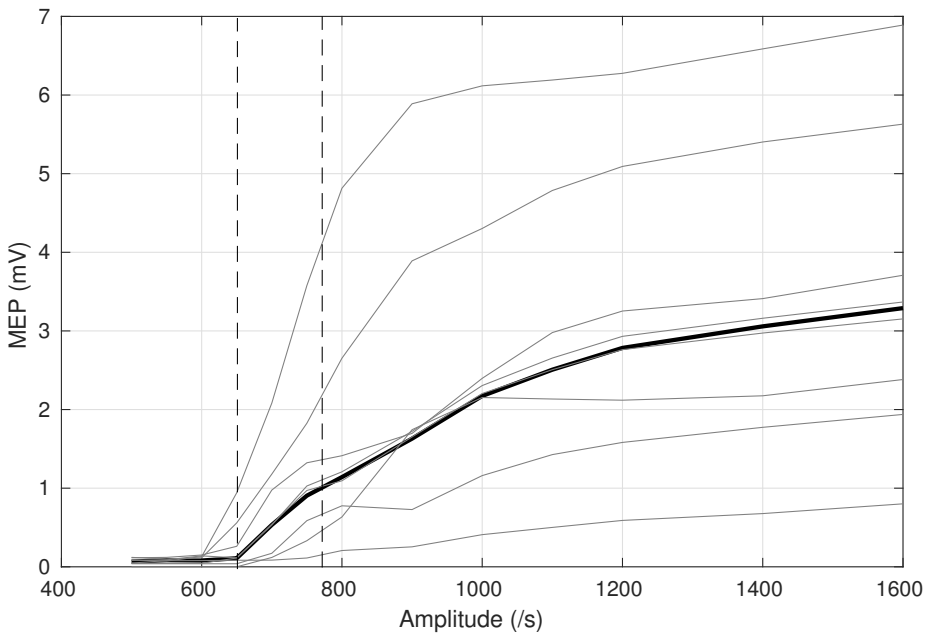

Figure 3: The size of the modeled MEP as a function of the stimulation intensity at rest. The black line denotes the standard parameter set; the eight gray lines show the responses for ±15% changes in each of the following parameters ν_{ex}, ν_{ee}, θ_v and $T_{\min}$. The dashed lines indicate RMT and 120%RMT.

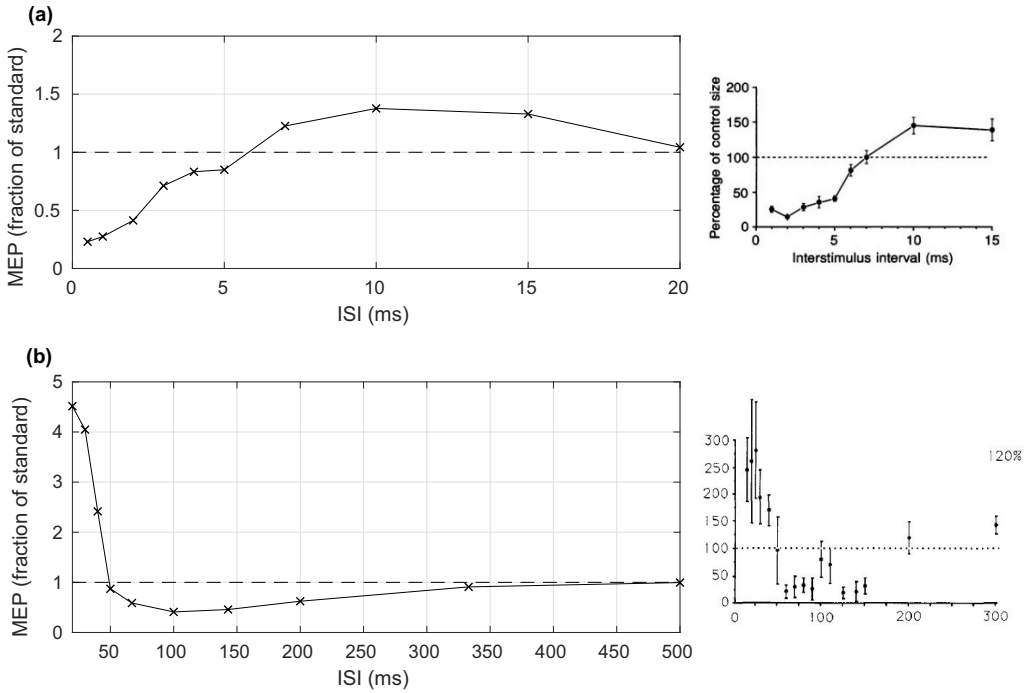

Figure 4: The modeled MEP changes as a result of paired-pulse protocols. MEPs are normalized in terms of the amplitude for a single test pulse and are plotted against the time between the two pulses, that is the ISI. (a) A 70% RMT conditioning pulse with a 120% test pulse demonstrates SICI and ICF. The results of [39] are shown in the right hand panel with permission. (b) A 120% RMT conditioning pulse with a 120% RMT test pulse shows LICI. The dashed lines indicate no change in MEP; a response above the line indicates facilitation, a response below indicated inhibition. The results of [40] are shown in the right hand panel with permission.

of LICI lasts to longer ISI (about 300 ms) than is typically seen experimentally (about 200 ms). Also, the modeled LICI is not as strong; MEPs are reduced in the model to around 40% of their baseline whereas in experiment they can be almost eliminated.

Next, we simulated the effect of GABAergic and anti-glutamatergic drugs on SICI, ICF, and LICI by modulating the coupling strengths between layer 2/3 cortical populations. Fig. 5(a) shows the effect of increasing the coupling strength due to $GABA_A$ receptors from the inhibitory to the excitatory population on SICI and ICF (equivalent to applying a $GABA_A$ agonist). The plot shows that increasing neurotransmission of $GABA_A$ receptors on excitatory populations increases SICI but reduces ICF. This agrees with experiment [41] which shows that a $GABA_A$ receptor agonist such as Diazepam increased SICI [42, 43, 44] but reduced ICF [45, 46].

Fig. 5(b) shows the effect of decreasing excitatory to excitatory coupling strength (equivalent to applying an anti-glutamatergic drug) on SICI and ICF. The plot shows that SICI is increased, whereas ICF is reduced by decreasing excitatory coupling, largely in agreement with studies applying anti-glutamatergic drugs such as Mematine [47] or Riluzole [48, 49], and NMDA-antagonists such as Amantadine [50] or Dextromethorphan.

Finally, we simulated the effect of increasing the inhibitory to excitatory coupling due to $GABA_B$ receptors (equivalent to applying a $GABA_B$ receptor agonist) on LICI. Figure 5(c) demonstrates a significant increase in LICI (ISI of 100 ms; two suprathreshold pulses) with increased $GABA_B$ receptor coupling to excitatory populations, again in agreement with experiments using $GABA_B$ receptor agonists such as baclofen [51]. Taken together, these findings demonstrate that our MEP model is able to capture a large range of paired-pulse TMS phenomena that are observed experimentally, including the effects of altering excitatory and inhibitory neurotransmission using different drugs.

3.3. Motor evoked potential during contraction

Figure 6(a) show the EMG response following a single pulse at 120% RMT and10% MVC. The background activity has resulted in a 10% increase in the amplitude of the MEP during a contraction. Also, a silent period is evident after the pulse during which there is no EMG, with background EMG returning after 300 ms. Further increasing the strength of the muscle contraction resulted in increased MEP amplitude, as shown in Fig. 6(b), in line with experimental findings.

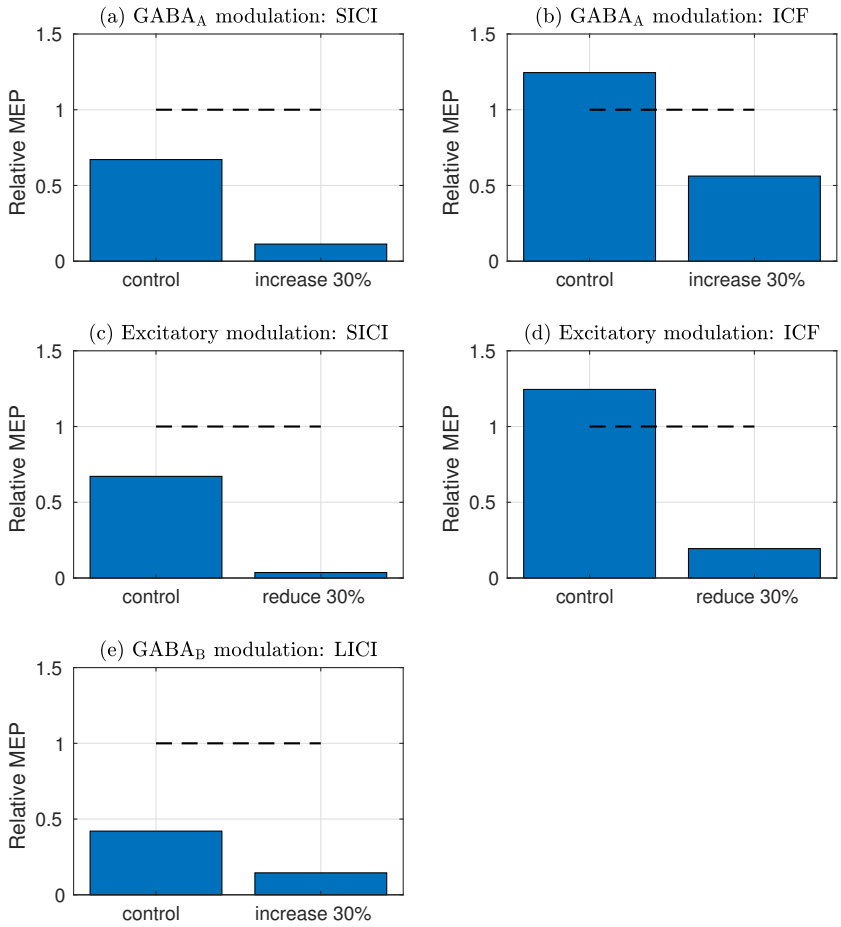

Figure 5: The effect of modulating couplings between populations on SICI (3 ms ISI), ICF (15 ms ISI) and LICI (100 ms ISI). (a) Modulating the GABA$_A$ inhibitory coupling to the excitatory population on SICI. The fractional change in modeled MEP (compared with a single test pulse) is plotted for two cases of the strength of the GABA$_A$to-excitatory coupling, ν_{ei}^{A}; specifically a 'control' value of (-0.72×10^{-4} V s) and a 30% increase (that is, 30% more negative) in this value. The dashed line indicates no change in MEP. (b) The same modulation as (a), but on ICF. (c) Modulating the excitatory to excitatory coupling on SICI. The 'control' corresponds to a coupling strength ν_{ee} of 1.92×10^{-4} V s, a 30% reduction in this value is also shown. (d) As (c), but for ICF. (e) Modulating the GABA$_B$ inhibitory coupling to the excitatory population on LICI. The 'control' corresponds to a relative coupling strength ν_{ie}^{B} of -0.72×10^{-4} V s; also shown is a 30% increase (i.e. 30% more negative) in this value.

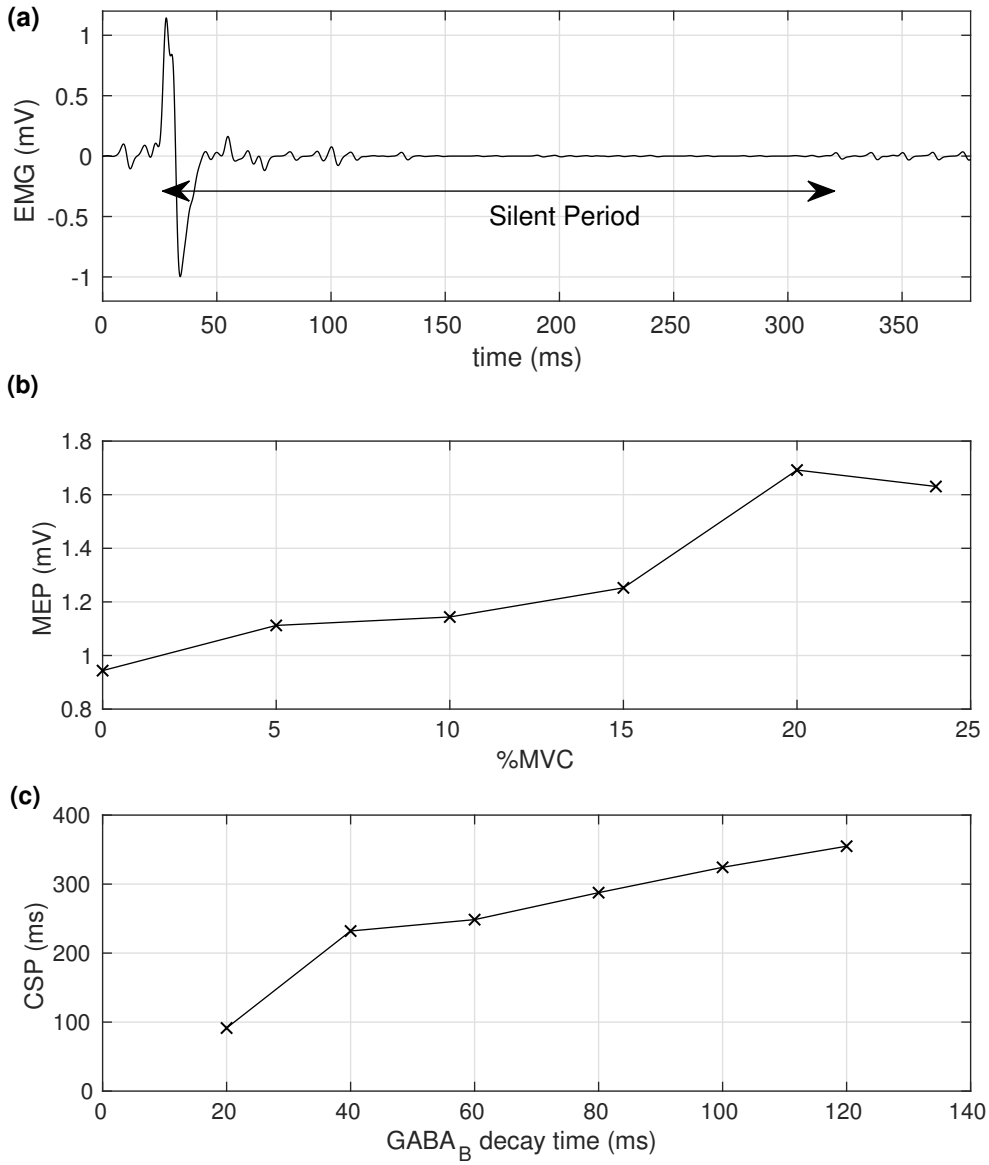

Figure 6: Modeled MEPs with muscle contraction. (a) The timecourse of the EMG at 120% RMT intensity and 10% MVC. The silent period is indicated. (b) The amplitude of the MEP as a function of muscle contraction (%MVC). (c) The duration of the silent period as a function of $GABA_B$ decay time constant.

Figure 6(c)shows the CSP against the time constant of the decay of $GABA_B$. As decay constant increases, the silent period also increases. This agrees with experimental results, but overall the modeled CSP is somewhat longer than typical measured CSPs [24]. The CSP reflects the long period in which the layer 5 pulse rate (Fig. 2(b)) drops below its equilibrium value due to build-up of $GABA_B$ and its length is strongly related to the timescale of $GABA_B$ decay [14].

3.4. Theta-burst stimulation

Having established that our model captures a wide range of single and paired pulse TMS phenomena, we next assessed whether modeled MEPs were sensitive to changes in synaptic weights induced following iTBS and cTBS predicted by a model of CaDP with metaplasticity. We searched across a range of parameter values mimicking variability in how TMS interacts with cortical circuits (TMS-e coupling) and variability in glutamatergic neurotransmission (e-e coupling). Figure 7 shows the predicted changes in MEPs following both cTBS and iTBS. There are several notable features to these outcomes. First, there are several areas within the parameter space that predict the 'canonical response to TBS (i.e. cTBS decreases MEPs, iTBS increases MEPs, e.g. the point $\circ$). Second, a wide variability in response profile can also be generated by altering how TMS interacts with cortical circuits (TMS-e coupling) and how excitatory populations interact with each other (e-e coupling). For instance, the point $*$ shows an opposite to canonical response, the point $\bigtriangledown$ a parameter set where both paradigms decrease MEP amplitude, and $\bigtriangleup$ a parameter set where both paradigms increase MEPs. Furthermore, there are parameter spaces where neither paradigm has a strong effect on MEP amplitude (e.g. 'non-responders'). The maximum predicted increase in MEPs ($\sim$1.15) is smaller in magnitude than the maximum predicted decrease ($\sim$0.7), and is also smaller than the maximum often observed in experiment ($\sim$1.8). Third, the response to TBS becomes unstable (i.e. locks in to a high firing rate similar to a seizure) at high values of both TMS-e coupling, but particularly e-e coupling, shown by the white space on Fig. 7. Interestingly, disorders associated with abnormal glutamatergic receptor function, such as anti-NMDA receptor encephalitis, are often accompanied by seizures. Fourth, the predicted changes in MEP amplitude following TBS across the parameter space are nonlinear — suggesting these relationships would not be evident with simple correlations often used in human TMS experiments. Taken together, these findings demonstrate

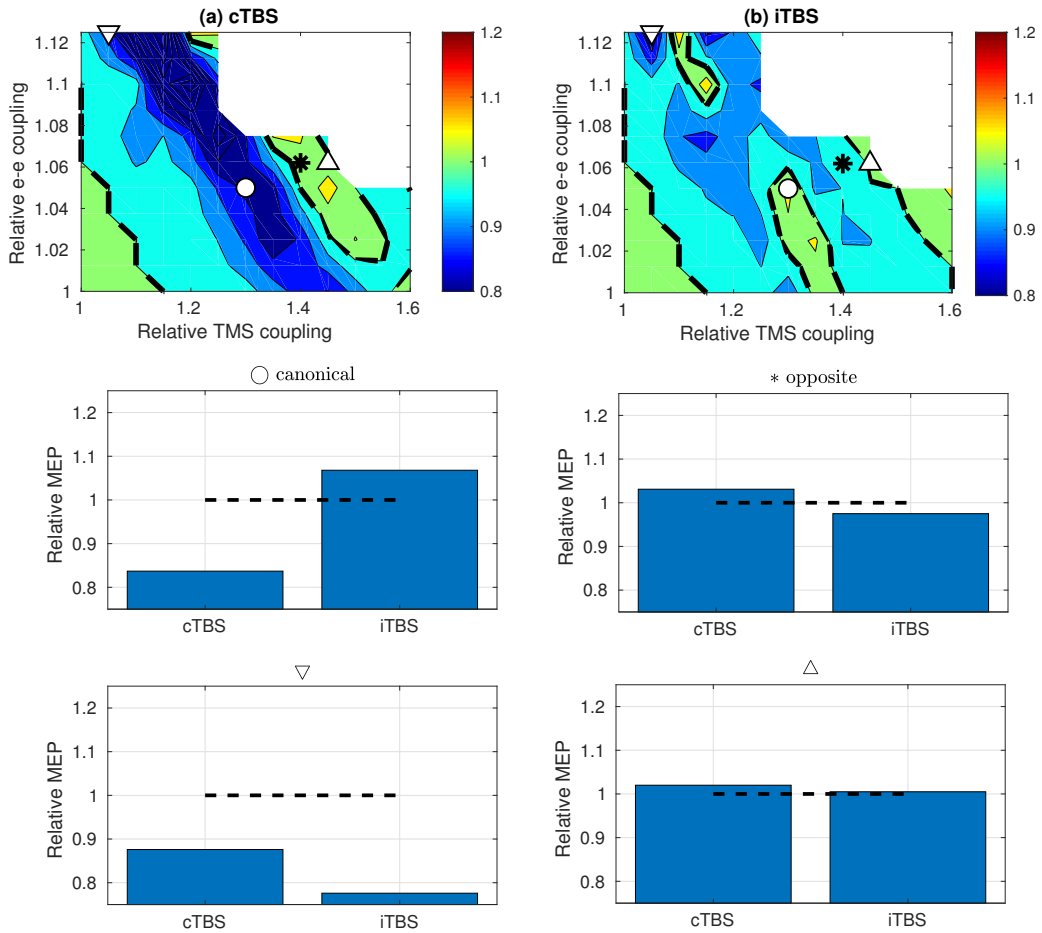

Figure 7: The modeled MEP changes as a result of (a) cTBS and (b) iTBS protocols against the relative strength of the TMS-to-excitatory coupling and excitatory-to-excitatory coupling strengths. The dashed lines show no change in synaptic weight. The weight changes at four points are indicated in the lower panels. A canonical response is indicated by ◯, an opposite-to-canonical response is indicated by $*$, both responses positive is indicated by △, and both responses negative by ▽.

that our MEP model is sensitive to changes in synaptic weight following TBS predicted by a model including rules for CaDP and metaplasticity, and is able to capture a variety of response profiles often observed in human TBS experiments.

4. Discussion

We have developed a biophysical model of MEPs following TMS to the motor cortex by combining a population-based model of cortical activity and an individual neuron model of motor output. The model captures many common features of MEPs including input-output characteristics, responses to paired-pulse paradigms, a silent period with voluntary contraction and changes in MEPs following plasticity-inducing TBS paradigms. It provide unique insights into how micro/mesoscale mechanisms, such as differences in synaptic weightings between excitatory/inhibitory neural populations, can impact TMS-evoked motor output and TMS-induced plasticity.

A limitation of our model is that it does not predict I-wave activity in layer 5 corticospinal neurons [13, 14]. Population-based models are not well suited for capturing highly synchronised events, such as I-waves, as mean population firing-rates are modeled instead of individual firing events. However, modeling at the population level is well suited for TMS [7], which simultaneously activates large neural populations, and captures the slower excitatory and inhibitory postsynaptic potentials that are likely involved in paired pulse phenomena. Indeed, our model is successful at capturing a wide range of single-pulse, paired-pulse and rTMS phenomena without explicitly modeling I-waves.

We have not considered trial-to-trial variability in MEP amplitude. MEP variability is likely driven by fluctuations in both cortical and spinal excitability [52]. An important next step will involve incorporating existing population-based models of cortical oscillations including cortico-thalamic loops [29] and more detailed models of spinal circuits. This approach will allow exploration of MEP variability, and allow modeling of TMS-evoked EEG activity [53].

Finally, we only qualitatively compared model predictions to real data. Future work assessing the capacity to predict unseen experimental data (e.g. following changes to a given parameter such as intensity or inter-stimulus interval) will help further define the predictive value of such models.

5. Conclusions

We have demonstrated how a biophysically plausible nonlinear model of MEPs can be combined with the output of a population-based model of cortical neurons in order to produce a description of MEPs due to TMS. The final MEP activity is realistic in terms of variation with intensity and muscle contraction, and demonstrates the known amplitude and interval-dependent effects in paired-pulse stimulation. The MEP model is also sensitive to changes in synaptic weight predicted by a model of TBS-induced plasticity including rules for CaDP and metaplasticity, demonstrating complex relationships between variability in methodological and biological factors and MEP changes following TBS. Overall, the approach allows population-based modeling of cortical plasticity using neural field theory to be better-interpreted, by providing a route by which the effect on the MEP can be evaluated. Continued development of such models in combination with human experiments will enable a unified theoretical understanding of how TMS interacts with and modifies cortical circuits.

Author statement

MTW constructed the model, carried out most of the modeling, and led the writing of the manuscript. BM provided guidance on the modeling approach. NCR provided experimental background and contributed to the manuscript. We declare no conflict of interest in this work. NCR is supported by an Australian Research Council DECRA fellowship (DE180100741).

Appendix A. The NFTsim model

The NFTsim model [23] uses a neural field approach to calculate population-averaged descriptions of neural behavior as a function of time and space. However, in this work we have excluded explicit spatial variation. Here we present briefly the model and its parameters.

The mean soma potential V_a of a population of neurons of type a ($a = e, i, v$) for layer 2/3 excitatory, layer 2/3 inhibitory, and layer 5 excitatory neurons respectively, is given by the sum of contributions from postsynaptic potentials (PSPs):

$$V_a(t) = \sum_b V_{ab}(t), \tag{A.1}$$

where V_{ab} describes the postsynaptic potential at the population a due to incoming events from population b ($b = e$, i, v, or x) where x describes an external stimulation due to TMS.

The time course of the PSPs is described by the dendritic response through the following equation:

$$\left(\frac{1}{\alpha_{ab}}\frac{d}{dt}+1\right)\left(\frac{1}{\beta_{ab}}\frac{d}{dt}+1\right)V_{ab}(t) = \nu_{ab}(t)\phi_{ab}(t-\tau_{ab}), \tag{A.2}$$

where α_{ab} and β_{ab} are rate constants for the rise and fall rates of the PSPs respectively, ν_{ab} is the strength of coupling, and ϕ_{ab} describes the rate of incoming axonal pulses, from cells of type b to cells of type a. The parameter τ_{ab} describes delay in propagation of signals from neurons of type a to type b; due to, for example, spatially long nerve pathways.

The mean firing rate of the population a is given by a sigmoidal function of the mean soma potential:

$$Q_a(V_a) = \frac{Q_a^{\max}}{1+e^{-(V_a-\theta_a)/\sigma_a}}, \tag{A.3}$$

where $Q_a^{\max}$ is the maximum firing rate, and θ_a is the threshold of the distribution and σ_a is proportional to the width of the sigmoid distribution.

Finally, the firing of the population a results in generation of axonal pulses, which propagate along axons towards synapses. This propagation is described by

$$\left(\frac{1}{\gamma_{ab}}\frac{d}{dt}+1\right)^2\phi_{ab}(t) = Q_{ab}(t), \tag{A.4}$$

where the parameters γ_{ab} represent the axonal propagation rates from neurons of type b to type a. Equations (A.1)–(A.4) describe the time-variation of quantities V_{ab}, V_a, Q_a and ϕ_{ab}, and are integrated forward in time to give the behavior of the neural populations.

To simplify, we assume that the dynamics depends only on the presynaptic cell, so that the subscript a on the parameters α_{ab}, β_{ab} and γ_{ab} is redundant; we label these parameters as α_b, β_b and γ_b respectively.

We include a superscript A or B on the synaptic inhibitory parameters to denote the $\mathrm{GABA_A}$ and $\mathrm{GABA_B}$ responses respectively. Furthermore, the multiple couplings from the layer 2/3 excitatory cells to the layer 5 cells are labelled with superscripts 'fast' and 'slow'.

The standard parameters for the description of the layer 2 and 3 excitatory and inhibitory cells have come from previous work [17, 22, 18, 30], and are listed in Table A.1. The layer 5 parameters have been chosen to give a plausible motoneuron output, consistent with Moezzi et al. [14], including a large maximum firing rate, but also with a low threshold for activation. The synaptic couplings to the layer 5 cells from the layer 2/3 cells have been tuned to show plausible behavior. The direct coupling from the TMS stimulation to the layer 5 cells is considerably lower than the indirect couplings from the layer 2/3 cells, reflecting the low amplitude of direct stimulation due to TMS deeper in the cortex. Time delays for the propagation to the layer 5 cells from the layer 2/3 cells are chosen to be consistent with Rusu et al. [13]; excitations far from the layer 5 soma requiring around 5 ms to travel to the soma. Others are commensurately quicker.

Appendix B. Calcium dependent metaplasticity

The equations and parameters for calcium dependent metaplasticity are presented briefly here; for full details see [22].

In the calcium-dependent plasticity (CaDP) scheme, the driver of plasticity is the postsynaptic intracellular calcium concentration $[\mathrm{Ca}^{2+}]_e$ (where e represents the excitatory layer 2/3 population in the current work), modulated through NMDA receptors [54]. The ultimate excitatory-to-excitatory synaptic weight $\tilde{\nu}_{ee}(t)$ is modeled through [22]

$$\frac{d\tilde{\nu}_{ee}}{dt} = \eta([\mathrm{Ca}^{2+}]_e)\left(\nu_{\max}\Omega([\mathrm{Ca}^{2+}]_e) - \tilde{\nu}_{ee}\right). \tag{B.1}$$

The $\tilde{\nu}_{ee}$ gives the value that the weight will ultimately come to when stimulation is stopped, thus it determines whether a protocol gives LTD or LTP. The parameter $\nu_{\max}$ gives the maximum possible weight; Ω is dimensionless parameter that depends on $[\mathrm{Ca}^{2+}]_e$ (0.5 for concentrations < 0.15 μM, 0 for concentrations between 0.15–0.5 μM and 1.0 at higher concentrations); η is a rate parameter that increases with increasing $[\mathrm{Ca}^{2+}]_e$

The actual synaptic weight ν_{ee} responds slower and is modeled through

$$\left(z\frac{d}{dt} + 1\right)^2 \nu_{ee} = \tilde{\nu}_{ee}. \tag{B.2}$$

where z is a characteristic response timescale.

Table A.1: The standard parameter values used in the NFTsim model [23] for the neural field modeling. The subscripts e, i and v denote layer 2/3 excitatory, layer 2/3 inhibitory and layer 5 populations respectively. We have used the simplification that γ_{ab}, α_{ab} and β_{ab} are dependent on only the presynaptic cell b; therefore only one subscript is used. The projections to the layer 5 cells are described with time delays τ_{vb} rather than axonal rate constants.

Parameter	Description	Value	Unit
Excitatory cells, dendrite responses and propagation rates			
α_e	dendritic rise rate	280	s^{-1}
β_e	dendritic fall rate	70	s^{-1}
γ_e	axonal rate	110	s^{-1}
θ_e	Mean threshold for excitatory firing	13×10^{-3}	V
σ_e	description of width of sigmoid distribution	3.8×10^{-3}	V
$Q_e^{\max}$	Maximum excitatory firing rate	340	s^{-1}
Inhibitory cells, dendrite responses and propagation rates			
α_i^{A}	dendritic rise rate to $\mathrm{GABA_A}$ input	400	s^{-1}
β_i^{A}	dendritic fall rate to $\mathrm{GABA_A}$ input	100	s^{-1}
α_i^{B}	dendritic rise rate to $\mathrm{GABA_B}$ input	40	s^{-1}
β_i^{B}	dendritic fall rate to $\mathrm{GABA_B}$ input	10	s^{-1}
γ_i	axonal rate	1000	s^{-1}
θ_i	Mean threshold for inhibitory firing	13×10^{-3}	V
σ_i	description of width of sigmoid distribution	3.8×10^{-3}	V
$Q_i^{\max}$	Maximum inhibitory firing rate	340	s^{-1}
Layer 5 cells			
θ_v	Mean threshold for excitatory firing	8×10^{-3}	V
σ_v	description of width of sigmoid distribution	2.5×10^{-3}	V
$Q_v^{\max}$	Maximum excitatory firing rate	900	s^{-1}
Synaptic couplings			
ν_{ee}	e-to-e synaptic coupling	1.92×10^{-4}	V s
ν_{ei}^{A}	$\mathrm{GABA_A}$-modulated i-to-e synaptic coupling	-0.72×10^{-4}	V s
ν_{ei}^{B}	$\mathrm{GABA_B}$-modulated i-to-e synaptic coupling	-0.72×10^{-4}	V s
ν_{ie}	e-to-i synaptic coupling	1.92×10^{-4}	V s
ν_{ii}^{A}	$\mathrm{GABA_A}$-modulated i-to-i synaptic coupling	-0.72×10^{-4}	V s
ν_{ii}^{B}	$\mathrm{GABA_B}$-modulated i-to-i synaptic coupling	-0.72×10^{-4}	V s
ν_{ve}^{fast}	fast e-to-v synaptic coupling	2.4×10^{-4}	V s
ν_{ve}^{slow}	slow e-to-v synaptic coupling	2.4×10^{-4}	V s
ν_{vi}^{A}	$\mathrm{GABA_A}$-modulated i-to-v synaptic coupling	-3.0×10^{-4}	V s
ν_{vi}^{B}	$\mathrm{GABA_B}$-modulated i-to-v synaptic coupling	-3.0×10^{-4}	V s
Propagation delays			
$\tau_{ve}^{\mathrm{fast}}$	fast e-to-v axonal delay	1×10^{-3}	s
$\tau_{ve}^{\mathrm{slow}}$	slow e-to-v axonal delay	5×10^{-3}	s
τ_{vi}	medium i-to$v$ axonal delay	3×10^{-3}	s
τ_{ie}^{A}	$\mathrm{GABA_A}$-modulated i-to-v axonal delay	3×10^{-3}	s
τ_{ie}^{B}	$\mathrm{GABA_A}$-modulated i-to-v axonal delay	3×10^{-3}	s
τ_{mv}	delay from v-to-motoneurons	20×10^{-3}	s

The postsynaptic calcium concentration $[\mathrm{Ca}^{2+}]_e$ itself depends on the glutamate binding and postsynaptic activity through

$$\frac{d[\mathrm{Ca}^{2+}]_e}{dt} = gB([\mathrm{glu}])H(V) - \frac{[\mathrm{Ca}^{2+}]_e}{\tau_{\mathrm{Ca}}}, \tag{B.3}$$

where g is the NMDA receptor-modulated calcium permeability, B is a sigmoidal function of the glutamate concentration [glu], H is voltage-dependent modulation of the dynamics (increasing with voltage V except at very high depolarizations), and τ_{Ca} a time-constant for calcium dynamics.

In the BCM approach to metaplasticity, the activity level that demarcates LTD from LTP is dependent on past activity. This is incorporated into CaDP by having conductance g dependent upon the history of the weight ν_{ee}:

$$\frac{dg}{dt} = \frac{1}{\tau_{\mathrm{rec}}}(g_0 - g) - \frac{g_0}{\tau_{\mathrm{BCM}}}\left(\frac{\tilde{\nu}_{ee}}{\nu_{ee}} - 1\right) \tag{B.4}$$

where g_0 is the calcium conductance at equilibrium, ν_{ee} is the actual synaptic weight, and $\tilde{\nu}_{ee}$ is the ultimate synaptic weight. The metaplasticity timescale is τ_{BCM} and the longer τ_{rec} is the recovery time for calcium conductance.

The glutamate concentration [glu] depends on presynaptic activity:

$$\frac{d[\mathrm{glu}]}{dt} = \lambda_{\mathrm{glu}}\phi_{ee} - \frac{[\mathrm{glu}]}{\tau_{\mathrm{glu}}}, \tag{B.5}$$

where λ_{glu} is the glutamate concentration released per presynaptic excitatory spike, ϕ_{ee} is the incoming synaptic from the excitatory population, Eq. (A.4), and τ_{glu} is the timescale for glutamate decay.

Equations (B.1) – (B.5), with functions η, Ω, B and H [55], represent CaDP with metaplasticity. The resulting ν_{ee} is fed back into Eq. (A.2). Parameters and functions for these equations are as defined in [55] and [22]; parameters are listed in Table B.2.

References

[1] Hallett M. Transcranial Magnetic Stimulation: A primer. Neuron. 2007;55:187–199.

[2] Ziemann U, Paulus W, Nitsche MA, Pascual-Leone A, Byblow WD, Berardelli A, et al. Consensus: motor cortex plasticity protocols. Brain stimulation. 2008;1(3):164–182.

Table B.2: Parameters for the calcium dependent metaplasticity model, taken from [55, 22].

Parameter	Description	Value	Unit
$\nu_{\max}$	Maximum synaptic coupling	10.0×10^{-4}	V s
λ_{glu}	Glutamate released per presynaptic excitatory spike	50×10^{-6}	M s
g_0	NMDAR-modulated Ca^{2+} conductance at equilibrium	2×10^{-3}	M s^{-1} V^{-1}
τ_{Ca}	Time-constant for calcium dynamics	50×10^{-3}	s
τ_{glu}	Time-constant for glutamate dynamics	30×10^{-3}	s
τ_{rec}	Timescale for recovery of calcium conductance	1000	s
τ_{BCM}	Timescale for metaplasticity	7	s
z	Characteristic timescale for synaptic strength induction	100	s

[3] Pascual-Leone A, Walsh V, Rothwell J. Transcranial magnetic stimulation in cognitive neuroscience–virtual lesion, chronometry, and functional connectivity. Current opinion in neurobiology. 2000;10(2):232–237.

[4] Lefaucheur JP, André-Obadia N, Antal A, Ayache SS, Baeken C, Benninger DH, et al. Evidence-based guidelines on the therapeutic use of repetitive transcranial magnetic stimulation (rTMS). Clinical Neurophysiology. 2014;125(11):2150–2206.

[5] Parkin BL, Ekhtiari H, Walsh VF. Non-invasive human brain stimulation in cognitive neuroscience: a primer. Neuron. 2015;87(5):932–945.

[6] Matheson NA, Shemmell JBH, De Ridder D, Reynolds JNJ. Understanding the effects of repetitive transcranial magnetic stimulation on neuronal circuits. Frontiers in Neural Circuits. 2016;10:67.

[7] Wilson MT, Fulcher BD, Fung PK, Robinson PA, Fornito A, Rogasch NC. Biophysical modeling of neural plasticity induced by transcranial magnetic stimulation. Clinical Neurophysiology. 2018;129:1230–1241.

[8] Thielscher A, Optiz A, Windhoff M. Impact of the gyral geometry on the electric field induced by transcranial magnetic stimulation. NeuroImage. 2010;54:234–243.

[9] Deng ZD, Lisanby SH, Peterchev AV. Electric field depth-focality trade-off in transcranial magnetic stimulation: Simulation comparison of 50 coil designs. Brain Stimulation. 2013;6(1):1–13.

[10] Opitz A, Legon W, Rowlands A, Bickel WK, Paulus W, Tyler WJ. Physiological observations validate finite element models for estimating subject-specific electric field distributions induced by transcranial magnetic stimulation of the human motor cortex. Neuroimage. 2013;81:253–264.

[11] Tang AD, Lowe AD, Garrett AR, Woodward R, Bennett W, Canty AJ, et al. Construction and evaluation of rodent-specific rTMS coils. Frontiers in Neural Circuits. 2016;10:47.

[12] Bungert A, Antunes A, Espenhahn S, Thielscher A. Where does TMS stimulate the motor cortex? Combining electrophysiological measurements and realistic field estimates to reveal the affected cortex position. Cerebral Cortex. 2016;1–12.

[13] Rusu CV, Murakami M, Ziemann U, Triesch J. A model of TMS-induced I-waves in motor cortex. Brain Stimulation. 2014;7:401–414.

[14] Moezzi B, Schaworonkow N, Plogmacher L, Goldsworthy MR, Hordacre B, McDonnell MD, et al. Simulation of electromyographic recordings following transcranial magnetic stimulation. Journal of Neurophysiology. 2017;120:2532–2541.

[15] Deco G, Jirsa VK, Robinson PA, Breakspear M, Friston K. The dynamic brain: from spiking neurons to neural masses and cortical fields. Public Library of Science Computational Biology. 2008;4(8):e1000092.

[16] Pinotsis D, Robinson P, beim Graben P, Friston K. Neural masses and fields: modeling the dynamics of brain activity. Frontiers in computational neuroscience. 2014;8:149.

[17] Fung PK, Haber AL, Robinson PA. Neural field theory of plasticity in the cerebral cortex. Journal of Theoretical Biology. 2013;318:44–57.

[18] Wilson MT, Fung PK, Robinson PA, Shemmell J, Reynolds JNJ. Calcium dependent plasticity applied to repetitive transcranial magnetic

stimulation with a neural field model. Journal of Computational Neuroscience. 2016;49:107–125.

[19] Li X, Rymer WZ, Zhou P. A simulation based analysis of motor unit number index (MUNIX) technique using motoneuron pool and surface electromyogram models. IEEE Transactions in Neural Systems Rehabilitation Engineering. 2012;20:297–304.

[20] Goetz SM, Alavi SMM, Deng Z, Peterchev AV. Statistical Model of Motor-Evoked Potentials. IEEE Transactions on Neural Systems and Rehabilitation Engineering. 2019;27(8):1539–1545.

[21] Huang YZ, Rothwell JC, Chen RS, Lu CS, Chuang WL. The theoretical model of theta burst form of repetitive transcranial magnetic stimulation. Clinical Neurophysiology. 2011;122(5):1011–1018.

[22] Fung PK, Robinson PA. Neural field theory of synaptic metaplasticity with applications to theta burst stimulation. Journal of Theoretical Biology. 2014;340:164–176.

[23] Sanz-Leon P, Robinson PA, Knock SA, Drysdale PD, Abeysuriya RG, Fung C P K Rennie, et al. NFTsim: Theory and simulation of multiscale neural field dynamics. PLoS Computational Biology. 2017;14:e1006387.

[24] Li B, Virtanen JP, Oeltermann A, Schwarz C, Giese MA, Ziemann U, et al. Lifting the veil on the dynamics of neuronal activities evoked by transcranial magnetic stimulation. eLife. 2017;6:e30552.

[25] Wright JJ, Liley DTJ. Dynamics of the brain at global and microscopic scales: Neural networks and the EEG. Behavioral and Brain Sciences. 1996;19:285295.

[26] Robinson PA, Rennie CJ, Wright JJ. Propagation and stability of waves of electrical activity in the cerebral cortex. Phys Rev E. 1997;56:826–840.

[27] Breakspear M. Dynamic models of large-scale brain activity. Nature Neuroscience. 2017;20:340–352.

[28] Funke K, Benali A. Cortical cellular actions of transcranial magnetic stimulation. Restorative Neurology and Neuroscience. 2010;28:399–417.

[29] Robinson PA, Rennie CJ, Rowe DL, O'Connor SC. Estimation of multiscale neurophysiologic parameters by electroencephalographic means. Human Brain Mapping. 2004;23(1):53–72.

[30] Wilson MT, Goodwin DP, Brownjohn PW, Shemmell J, Reynolds JNJ. Numerical modelling of plasticity induced by transcranial magnetic stimulation. Journal of Computational Neuroscience. 2014;36:499–514.

[31] Di Lazzaro V, Profice P, Ranieri F, Capone F, Dileone M, Olivero F A Pilato. I-wave origin and modulation. Brain Stimulation. 2012;5:512–525.

[32] Wilson MT, Robinson PA, O'Neill B, Steyn-Ross DA. Complementarity of spike- and rate-based dynamics of neural systems. PLoS Computational Biology. 2012;8:e1002560.

[33] Ziemann U, Rothwell JC, Ridding MC. Interaction between intracortical inhibition and facilitation in human motor cortex. The Journal of physiology. 1996;496(3):873–881.

[34] Devanne H, Lavoie BA, Capaday C. Input-output properties and gain changes in the human corticospinal pathway. Experimental Brain Research. 1997;114:329–338.

[35] Olmo G, Laterza F, Lo Presti L. Matched wavelet approach in stretching analysis of electrically evoked surface EMG signal. Signal Processing. 2000;80:671–684.

[36] Hamada M, Murase N, Hasan A, Balaratnam M, Rothwell JC. The role of interneuron networks in driving human motor cortical plasticity. Cerebral Cortex. 2013;23:1593–1605.

[37] Mori F, Ribolsi M, Kusayanagi H, Siracusano A, Mantovani V, Marasco E, et al. Genetic variants of the NMDA receptor influence cortical excitability and plasticity in humans. Journal of Neurophysiology. 2011;106(4):1637–1643.

[38] Romero MC, Davare M, Armendariz M, Janssen P. Neural effects of transcranial magnetic stimulation at the single-cell level. Nature Communications. 2019;10:2642.

[39] Kujirai T, Caramia MD, Rothwell JC, Day BL, Thompson PD, Ferbert A, et al. Corticocortical inhibition in human motor cortex. Journal of Physiology. 1993;471:501–519.

[40] Valls-Solé J, Pascual-Leone A, Wassermann EM, Hallett M. Human motor evoked responses to paired transcranial magnetic stimuli. Electroencephalography and Clinical Neurophysiology/Evoked Potentials Section. 1992;85(6):355–364.

[41] Ziemann U, Reis J, Schwenkreis P, Rosanova M, Strafella A, Badawy R, et al. TMS and drugs revisited 2014. Clinical Neurophysiology. 2015;126:1847–1868.

[42] Di Lazzaro V, Pilato F, Dileone M, Tonali PA, Ziemann U. Dissociated effects of diazepam and lorazepam on short-latency afferent inhibition. The Journal of Physiology. 2005;569(1):315–323.

[43] Lazzaro VD, Pilato F, Dileone M, Profice P, Ranieri F, Ricci V, et al. Segregating two inhibitory circuits in human motor cortex at the level of GABAA receptor subtypes: A TMS study. Clinical Neurophysiology. 2007;118(10):2207 – 2214.

[44] Müller-Dahlhaus JFM, Liu Y, Ziemann U. Inhibitory circuits and the nature of their interactions in the human motor cortex a pharmacological TMS study. The Journal of Physiology. 2008;586(2):495–514.

[45] Inghilleri M, Berardelli A, Marchetti P, Manfredi M. Effects of diazepam, baclofen and thiopental on the silent period evoked by transcranial magnetic stimulation in humans. Experimental Brain Research. 1996;109(3):467–472.

[46] Mohammadi B, Krampfl K, Petri S, Bogdanova D, Kossev A, Bufler J, et al. Selective and nonselective benzodiazepine agonists have different effects on motor cortex excitability. Muscle & Nerve. 2006;33(6):778–784.

[47] Schwenkreis P, Witscher K, Janssen F, Addo A, Dertwinkel R, Zenz M, et al. Influence of the N-methyl-d-aspartate antagonist memantine on human motor cortex excitability. Neuroscience Letters. 1999;270(3):137 – 140.

[48] Schwenkreis P, Liepert J, Witscher K, Fischer W, Weiller C, Malin JP, et al. Riluzole suppresses motor cortex facilitation in correlation to its plasma level. Experimental Brain Research. 2000;135(3):293–299.

[49] Liepert J, Schwenkreis P, Tegenthoff M, Malin JP. The glutamate antagonist Riluzole suppresses intracortical facilitation. Journal of Neural Transmission. 1997;104(11):1207–1214.

[50] Reis J, John D, Heimeroth A, Mueller HH, Oertel WH, Arndt T, et al. Modulation of human motor cortex excitability by single doeses of amantadine. Neuropsychopharmacology. 2006;31:2758–2766.

[51] McDonnell MN, Orekhov Y, Ziemann U. The role of GABAB receptors in intracortical inhibition in the human motor cortex. Experimental Brain Research. 2006;173(1):86–93.

[52] Kiers L, Cros D, Chiappa KH, Fang J. Variability of motor potentials evoked by transcranial magnetic stimulation. Electroencephalography and Clinical Neurophysiology/Evoked Potentials Section. 1993;89(6):415–423.

[53] Rogasch NC, Fitzgerald PB. Assessing cortical network properties using TMS-EEG. Human Brain Mapping. 2013;34(7):1652–1669.

[54] Shouval HZ, Bear MF, Cooper LN. A unified model of NMDA receptor-dependent bidirectional synaptic plasticity. Proceedings of the National Acadamy of Sciences. 2002;99:10831–10836.

[55] Fung PK, Robinson PA. Neural field theory of calcium dependent plasticity with applications to transcranial magnetic stimulation. Journal of Theoretical Biology. 2013;324:72–83.